ACS OMEGA

Open Access

http://pubs.acs.org/journal/acsodf

Article

Rapid Whole-Plate Cell and Tissue Micropatterning Using a Budget 3D Resin Printer

Anamika Singh,[#] Youn Kyoung Cho,[#] and Daniel J. Cohen*

Cite This: *ACS Omega* 2024, 9, 43808−43816

Read Online

ACCESS | Metrics & More | Article Recommendations | Supporting Information

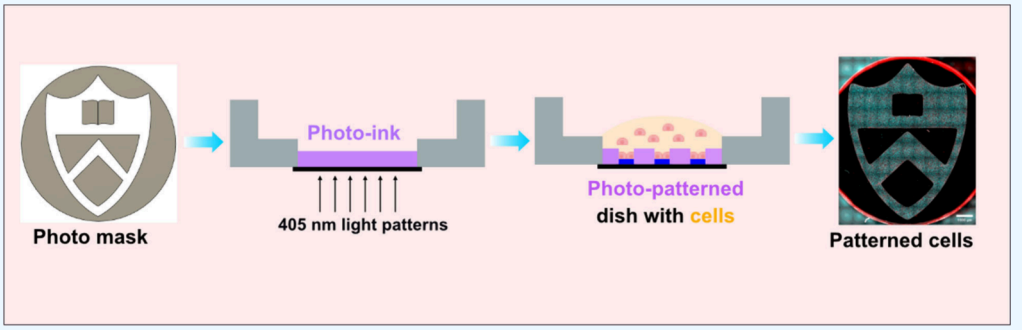

ABSTRACT: The ability to precisely pattern cells and proteins is crucial in various scientific disciplines, including cell biology, bioengineering, and materials chemistry. Current techniques, such as microcontact stamping, 3D bioprinting, and direct photopatterning, have limitations in terms of cost, versatility, and throughput. In this Article, we present an accessible approach that combines the throughput of photomask systems with the versatility of programmable light patterning using a low-cost consumer LCD resin printer. The method involves utilizing a bioinert hydrogel, poly(ethylene glycol) diacrylate (PEGDA), and a 405 nm sensitive photoinitiator (LAP) that are selectively cross-linked to form a hydrogel upon light exposure, creating specific regions that are protein and cell-repellent. Our result highlights that a low-cost LCD resin printer can project virtual photomasks onto the hydrogel, allowing for reasonable resolution and large-area printing at a fraction of the cost of traditional systems. The study demonstrates the calibration of exposure times for optimal resolution and accuracy and shape corrections to overcome the inherent challenges of wide-field resin printing. The potential of this approach is validated through widely studied 2D and 3D stem cell applications, showcasing its biocompatibility and ability to replicate complex tissue engineering patterns. We also validate the method with a cell-adhesive polymer (gelatin methacrylate; GelMA). The combination of low cost, high throughput, and accessibility makes this method broadly applicable across fields for enabling rapid and precise fabrication of cells and tissues in standard laboratory culture vessels.

1. INTRODUCTION

The ability to create precise patterns of cells and proteins based on flat culture surfaces is now a mainstay technique across cell biology,[1,2] bioengineering and biotechnology,[3] and materials chemistry.[4,5] These patterns are valuable both for allowing unique geometries to be created, such as for tissue engineering,[6] and for massively increasing throughput for parameter sweeps and statistical power.[7] The most common patterning approach today remains microcontact stamping, essentially using a microscale rubber stamp pattern to transfer a reagent to a substrate over macroscopic areas.[8] While standard, microcontact stamping typically requires a full-stack cleanroom process to produce the master mold from which the stamps are cast, meaning patterns cannot be changed without another cleanroom process, and each stamp typically has a finite lifetime and limited yield. The time-, expertise-, and equipment-intensive processes can be a barrier to entry. More recently, direct photopatterning techniques have become more common for selective positioning of biomolecules such as cells and protein.[9] The process takes advantage of photoreactive chemistries to either create or uncage a passivated adhesive layer[10,11] using 254−405 nm light. Some of these processes require physical photomasks, but the masks cannot be changed, must often be made from quartz to transmit 254 nm UV light, and cannot be used to pattern substrates where the photomask does not fit.[12] Moreover, parallel processing requires duplicate masks. Dynamic photomasking systems such as digital mirror devices (DMDs) allow the projection of focused, near-UV light into a small region of a Petri dish to

Received: July 15, 2024
Revised: September 26, 2024
Accepted: October 2, 2024
Published: October 18, 2024

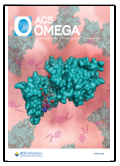

polymerize an inert hydrogel (poly(ethylene glycol), PEG) that prevents cells or proteins from attaching wherever it is polymerized.[13−15] While versatile, such biotechnology DMD setups can run from ∼$3000 (DIY) to $20 000 (commercial), and these systems can only print in relatively small areas (∼10 cm^2), significantly reducing throughput and substrate choices. The cost and limited throughput are both barriers to entry, and there is value to developing a more versatile and user-friendly platform where the goal is to have reasonable resolution, large-area 2D patterning, and low cost.[16]

Our approach is not intended to compete with commercial 3D bioprinters but rather to combine the throughput of photomask systems with the versatility of programmable light patterning systems to create a low-cost approach that can be used to create 2D micropatterns across a range of standard laboratory substrates from 3.5 cm Petri dishes to full 96-well high-throughput plates at a cost ∼10−30× lower than current DIY or commercial systems (Figure 1) while providing significant ease-of-use. Our method harnesses two recent technological trends: (1) the rise of low-cost hobby 3D resin printers and (2) the availability of high-resolution monochrome liquid-crystal displays (LCDs) that can be placed in front of a light-emitting-diode (LED) array to project patterns of light. Monochrome LCDs allow efficient transmission of 405 nm light, which is needed for certain photochemistries, a relatively precise voxel size (∼35 μm), and a massive working area of more than ∼100 cm^2 (large enough for all standard laboratory plates). Here, we demonstrate how effectively a low-cost consumer LCD printer (∼$350) can perform for common biotechnology patterning assays based on polymerizing an inert PEG resin wherever we want to prevent cell or protein attachment. Specifically, we were able to achieve reliable cell patterning with array features down to ∼300 μm simultaneously patterned over an area the size of a 96-well plate, even with sensitive models such as 3D stem cell differentiation.

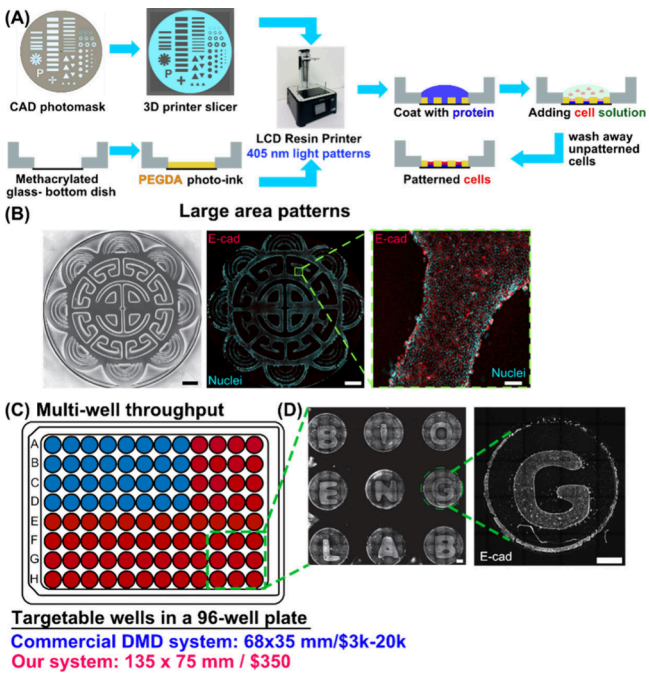

Figure 1. LCD resin printer strategy for protein and cell patterning. (A) Schematic representation of protein and cell patterning using a resin printer. A 405 nm light is projected from the monochrome LCD screen of the resin printer with uploaded virtual photomasks. Photo-cross-linked PEGDA500 renders the surface protein and cell repellent, while unprojected areas are washed and exposed for extracellular matrix protein and cell patterning. (B) Phase-contrast image of fully patterned wells on a 3.5 cm glass-bottomed Petri dish (left). Epifluorescence images of patterned Ecad:dsRed-expressing MDCK cells and their nuclei (center, right). Scale bars: 2 mm (left, center) and 100 μm (right). (C) Comparison of the projection area of the LCD resin printer (red) and the average DMD (blue) to the size of a 96-well plate (left). (D) Epifluorescence images of patterned Ecad:dsRed-expressing MDCK cells in a 3 × 3 array of wells in a 96-well plate (center) and a zoomed-in image of one well (right). Scale bars: 1 mm.

2. MATERIALS AND METHODS

2.1. Acrylate Functionalization of Glass-Bottomed Dishes for Gel Adhesion. Functionalizing glass substrates with acrylate groups will covalently attach polymerized poly(ethylene glycol) diacrylate (PEGDA) gel layers and prevent the gel from floating away during later use.[17] Briefly, for silanization, we prepared a silane solution by mixing 20 mL of ethanol (459844, Sigma-Aldrich), 1 mL of 3-(trimethoxysilyl) propyl-methacrylate (440159, Sigma-Aldrich) and 0.5 mL of dilute acetic acid (1:10 v/v solution of acetic acid (A6283, Sigma-Aldrich) in Milli-Q water). Respectively, 2 mL and 100 μL of the silanizing solution was added to the wells of a glass-bottomed 3.5 cm dish (D35-20-1.5-N, Cellvis) and 96-well plate (P96-1.5H-N, Cellvis). The vessels were covered, parafilmed, and incubated for 12−24 h at room temperature in a chemical hood. The dishes were then washed with an excess of ethanol and incubated for 5 h at 60 °C. This is the longest step in the whole process, but many dishes can be functionalized at one time. The total hands-on time for silanization is approximately 15 min (most of it is incubation). After the incubation step, the dishes could be used directly or stored at 4 °C in the dark up to 8 weeks for further use.

2.2. Preparation of the PEGDA Micropatterns. We used a Phrozen Mini 4K resin printer (Phrozen) to make all photopatterns. PEGDA500 photoink was purchased from Cellink and used as received. The CAD designs for the micropatterns were made using Fusion360 software, the files were saved in .stl format, and the virtual photomasks were generated by extruding the design where the light needed to be exposed. The .stl file was sliced using Chitubox (slicing software). In Chitubox, we set the bottom layer thickness as "1" and exposure time as 40, 70, or 100 s accordingly. For micropatterning in 3.5 cm dishes, we added 300 μL of the PEGDA500 photoink in the center of the methacrylated glass bottom dish to make a flat layer. The z-axis plate of the resin printer was removed, and the dish was kept in the center of the printer. The patterns were made using different exposure times such as 40, 70, and 100 s, washed using PBS until all the unpolymerized resin was removed, and then stored in pure PBS at 4 °C until use. This step can take more time with multiwell plates, but multichannel pipettes can mitigate this.

2.3. LCD Screen Power Measurements. The power of the LCD screen was measured with a power meter (PM200, Thorlabs) that was set for a wavelength of 405 nm. Fifteen sections of the screen were measured three times each and averaged to determine the average intensity and uniformity.

2.4. Characterization of the PEGDA Micropatterns. To measure the dimensions of the micropatterns, the hydrogels were incubated with red fluorescent beads to allow the beads to coat the gel surface. The fluorescent beads (F8810,

https://doi.org/10.1021/acsomega.4c06539
ACS Omega 2024, 9, 43808−43816

FluoSpheres) were mixed with PBS in a ratio of 1:50 (v/v). The hydrogels were incubated with the fluorescent beads for 48−72 h at 4 °C. Epifluorescence and phase-contrast images of the micropatterns were captured using a 4× phase contrast objective on a Nikon Ti2 microscope. We measured dimensions and features using ImageJ/FIJI software. Briefly, fluorescence images were binarized and measured with line profiles and automatic bounding boxes to determine key 2D dimensions. 3D measurements were made from XZ resliced Z-stacks of confocal images captured with a Nikon Ti2-NL5 confocal or a Leica SPE scanning confocal microscope.

2.5. Preparation of GelMA Micropatterns. We purchased GelMA (PhotoGel-INK) from Cellink and used it as indicated by the manufacturer. The photoink was heated at 37 °C in the water bath for 20 min. The methacrylated glass bottom dish was kept at 37 °C inside an incubator to keep it warm before printing. For GelMA micropatterning, we added 600 μL of photoink in the center of the dish. The patterns were made using a 70 s exposure time. To remove the un-cross-linked GelMA, micropatterns were washed multiple times with warm PBS (37 °C). The dish was kept in an incubator at 37 °C, and the PBS was changed at least 3 times within 24 h to remove all traces of un-cross-linked resin. The GelMA micropatterns in PBS were stored at 4 °C until use.

2.6. Cell Maintenance. All cells were grown in an incubator at 37 °C and 5% CO_2 in humidified air. Large-scale tissue patterning was performed with MDCK-II cells that stably expressed Ecad:dsRed. The MDCK cell line was cultured in low glucose Dulbecco's Modified Eagle's Medium with phenol red (D5523-10L, Sigma) supplemented with 1 g/L sodium bicarbonate (S5761-500G, Sigma), 10% (v/v) fetal bovine serum (S11550, Atlanta Biologicals), and 1% (v/v) streptomycin/penicillin (15140-122, Gibco). 2D and 3D stem cell patterning experiments were performed with the mEGFP E-cadherin-labeled WTC-11 hiPSC lines from the Allen Institute. hiPSC lines were maintained in feeder-free maintenance mTeSR1 basal medium supplemented with 5X Supplement (85850, StemCell Technologies). Cells were routinely passaged and cultured on the plastic tissue culture plate coated with growth factor-reduced Matrigel (356231, Corning). Coating was performed for 1 h at room temperature or at 4 °C for long-term storage, up to 2 weeks.

2.7. Cell Seeding on Micropatterns. PEGDA-printed dishes were first sterilized before cell attachment by exposure to UV light in the tissue culture hood while the printed pattern was submerged once with 70% ethanol in DI water and twice in PBS with 1% streptomycin/penicillin. After sterilization, dishes were washed three times with PBS and coated with appropriate extracellular matrix proteins. For MDCK cell patterning, dishes with printed PEGDA structures were coated with 300 μL of collagen IV solution in PBS (C7521-5MG, Sigma; 50 ug/mL) overnight at 4 °C and further washed three times with DI water. MDCK cells were washed with PBS and detached from the culture plate by incubating cells in TrypLE (12604-013, Gibco) for 7 min at 37 °C. The cell solution was diluted with culture media and centrifuged at 1500 rpm for 3 min. After the supernatant was aspirated, the cell pellet was resuspended into the fresh media to acquire 2E6 cells/mL.

Similarly, GelMA patterns were seeded with MDCK cells. The dishes with GelMA patterns were coated with 600 μL of collagen IV solution (50 ug/mL) at 37 °C for 1 h to enhance cellular adhesion. We acquire a cell concentration of 3E6 cells/ml for cell seeding on GelMA patterns. Cells were cultured for 10 days until they formed the monolayer tissue, and the medium was changed every other day.

For hiPSC patterning, dishes were coated with laminin-521 (200−0117, StemCell Technologies; 20 ug/mL) in PBS with calcium and magnesium (PBS++) overnight at 4 °C and further washed three times with PBS++. hiPSCs were detached with warmed-up Accutase (A11105-01, Gibco) for 3 min at 37 °C. The cell solution was diluted in PBS and centrifuged at 1000 rpm for 3 min. Cell pellets were resuspended into the mTeSR media with 10 μM ROCK inhibitor (Ri) (72308, StemCell Technologies) to improve the cell viability in a single cell suspension.

The cell solution (300 uL) was seeded only to the glass part of the dish and placed in the incubator for 2 h at 37 °C. Then the dish was washed three times with PBS to remove the unattached cells and filled with 1700 μL of culture media to fill up the dish. For the pluripotency test, seeded cells were cultured in rock inhibitor (RI)-supplemented mTeSR media for 24 h and fixed for the OCT 3/4 stain.

2.8. Stem Cell Differentiation. For differentiation assays, hiPSC colonies were initially cultured in mTeSR with RI for 2 h after seeding. Then, RI was removed by replacing the media with warmed-up mTeSR. Three hours later, differentiation was performed by adding 50 ng/mL of recombinant human BMP-4 protein (314-BP, Biotechne) in mTeSR and culturing the sample for 42 h in the incubator. Tissue was then fixed for immunostaining and imaging.

2.9. 3D Lumen Formation. After seeding 300 μL of 1.1E6 cells/mL hiPSC cell solution into the laminin-coated micropatterns, we allowed cells to form a complete monolayer by culturing hiPSC colonies in mTeSR with Ri for 24 h in the incubator. After checking the micropattern was filled completely, we changed the media to ice-cold mTeSR with 4% Matrigel to allow the transition from 2D micropatterned monolayers to a 3D lumenized structure. After 24 h of culture in the incubator, the tissue was fixed for immunostaining and imaging.

2.10. Immunostaining. Tissues were washed twice with PBS and fixed with 4% (v/v) paraformaldehyde solution in PBS (15710, Electron Microscopy Science) for 15 min at room temperature. For fluorescently labeled cell lines, fixation and staining were all performed in dark conditions. Tissues were washed five times with PBS and permeabilized with 0.1% Triton-X-100 in PBS (T8787-100 ML, Sigma) for 15 min at room temperature. After being washed three times with 0.05% (v/v) Tween 20 in PBS (PBT), tissues were blocked with 1% bovine serum albumin (BSA; A1595-50 ML, Sigma) for 1 h at room temperature. The same blocking buffer was used to dilute the primary and secondary antibodies. Primary antibodies used for immunostaining were pSMAD 1/5 (1:300; MA5-15124, Invitrogen) and OCT3/4 (1:200; sc-5279, Santa Cruz). Secondary antibodies used for immunostaining were Alexa Fluor 555 donkey-antirabbit (1:500; A-31572, Invitrogen) and Alexa Fluor 647 goat-antimouse (1:500; A-21235, Invitrogen). Nuclear staining was performed by adding one standard drop of NucBlue Reagent81 (R37605, Invitrogen) to the secondary antibody solution. Nuclear staining was also performed using Hoechst 33342 nuclear stain (H3570, Invitrogen) according to manufacturer's protocol.

2.11. Microscopy. Phase contrast and epifluorescence images were acquired with an inverted Nikon Ti2 microscope using NIS Elements software and a Nikon Qi2 camera. Large images were obtained by selecting large image options in the

https://doi.org/10.1021/acsomega.4c06539
ACS Omega 2024, 9, 43808−43816

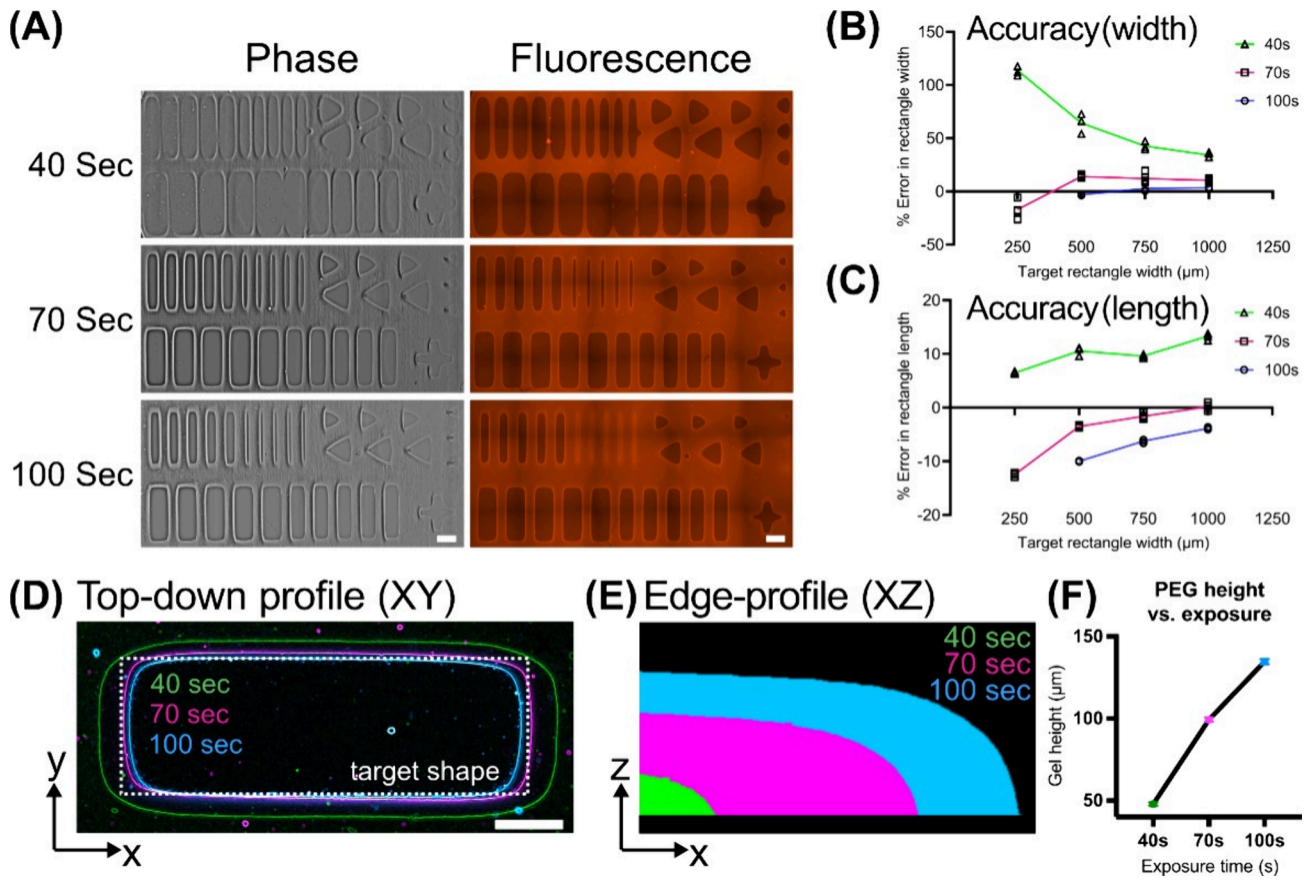

Figure 2. Effect of exposure time on patterned PEGDA hydrogel characteristics. (A) Phase-contrast (left) and epifluorescence (right) images of multiarray features, with five replicates, printed with exposure times of 40, 70, and 100 s (top, middle, and bottom, respectively). Epifluorescence images were acquired by depositing fluorescence beads on completed PEGDA hydrogel structures. Scale bars: 1 mm. (B) Percentage error from the target rectangle width for different exposure times. (C) Percentage error from the target rectangle length for different exposure times (n = 5). (D) Overlay of the XY top-down edge profile of representative rectangles printed with various exposure times. The white dotted line represents the targeted design size. Scale bar: 500 μm. (E) Overlay of the XZ edge profiles of representative structures printed with different exposure times. (F) Height of hydrogels printed with varying exposure times (n = 3).

software. The z-stacked fluorescence images were captured on a Leica SPE inverted confocal microscope using LAX software with a 561 nm laser, 10× objective, and 1 μm z-slice. 3D lumen imaging took place on Nikon Ti2-NL5 confocal with a 40× 1.25 silicone-immersion objective. GelMA micropatterns were imaged at the Princeton University Confocal Imaging Core Nikon Center using a Nikon Ti2 inverted microscope with a Yokogawa W1 spinning disk and SoRa module using the laser lines with 405 and 561 nm wavelengths by employing a 10× objective and 5 μm z-slice. For a large field of view, GelMa patterns were imaged on a Nikon Ti2-NL5 confocal microscope with a 2× objective.

3. RESULTS

3.1. Adapting an LCD Resin Printer for Cell and Protein Patterning. Our core strategy was to use patterns of light to photo-cross-link a layer of inert hydrogel wherever we did not want cells or proteins to adhere within in standard culture vessels (Petri dishes, multiwell plates, etc.) as shown in Figure 1. For this strategy, we chose a bioinert hydrogel that would cross-link upon proper exposure to light to physically mask specific regions of a culture plate. Anywhere not exposed to light would remain unmodified and available for cell culture. To reduce barriers to entry, we first chose to adopt a common and off-the-shelf chemistry using PEGDA chemistry. When PEGDA is combined with lithium phenyl-2,4,6-trimethylbenzoylphosphinate (LAP; a 405 nm sensitive photoinitiator), the acrylate groups cross-link the PEG and a bioinert gel forms. PEG has been the foundation for most antifouling and protein/cell patterning techniques, and PEGDA inks can be purchased preformulated with LAP or even synthesized in-house to dramatically reduce consumable costs.[18] For example, custom PEGDA-based photoinks have been synthesized by other groups and used to print microfluidics and organ-on-a-chip devices.[19]

As LAP enables PEGDA cross-linking in 405 nm light, we identified low-cost resin printers containing 405 nm light sources and down-selected from those to only consider monochrome LCD platforms (good 405 nm transmission) that would provide the combination of high-resolution, large printable area, and low cost (~$300). The most promising candidate was the Phrozen Mini 4K system, and the only modification needed to our chosen printer was to unscrew the Z-axis plate, as we are essentially using the 3D printer as a 2.5D printer to pattern a layer of PEGDA on a 2D substrate. Controlling this kind of system requires a simple modification to the standard 3D model file (CAD) design; here, the z-thickness in a CAD model corresponds to the effective local exposure time (see Materials and Methods). This strategy allows the researcher to use any standard 3D file generator

https://doi.org/10.1021/acsomega.4c06539
ACS Omega 2024, 9, 43808−43816

(e.g., Autodesk Fusion, Solidworks, SketchUp) while "tricking" the resin printer slicer software into thinking it is printing a 3D structure. Preparing the printing sample is also relatively simple. We first silanized glass-bottomed culture vessels with a methacrylate silane. This is optional but ensures strong bonding of the polymerized PEGDA to the dish floor. Next, we added sufficient PEGDA to cover the target area (e.g., 300 μL for a standard 3.5 cm glass-bottomed Petri dish) and then aligned the culture dish with where our printed pattern would be projected from the LCD. After a brief exposure, we removed the dish and washed it with deionized water. Finally, we backfilled the dish with an extracellular matrix protein (e.g., collagen) to ensure strong cell attachment, then seeded cells into the dish and allowed them to adhere. Interestingly, the unreacted methacrylate groups in the nonexposed areas did not seem to prevent extracellular matrix protein deposition or cell adhesion. It is possible that the unreacted methacrylate groups remain but are passive due to the lack of other acrylate groups to bind to. Also, the silane bonds in the nonexposed areas may hydrolyze over time, and the silanes may dissociate. The full workflow of this process of going from a CAD file to a patterned, inert hydrogel layer in a culture plate is shown in Figure 1A.

Several key advantages to using an LCD printer system for this application are immediately apparent . First, the large native area of an LCD printer means that very large and intricate single tissues can be created at scales far beyond traditional tissue micropatterning (e.g., single patterns spanning multiple centimeters) (Figure 1B). Second, unique patterns of living cells can be created in each well of a traditional multiwell plate, allowing compatibility with a wide range of standard commercial culture vessels to enable high-throughput biotechnology assays where many replicates or conditions are required (Figures 1C and D).

3.2. Characterizing Patterning Conditions and Accuracy. How well does this approach work in terms of accuracy and reproducibility? Photopolymerization chemistries depend on the photon flux, often controlled by varying the light intensity or exposure time. Commercial LCD printers have a fixed illumination intensity, but the effective exposure time can be chosen with the software. A perfectly collimated lithographic system will produce straight-sidewalls and dimensional accuracy, but low-cost resin printers are not perfectly collimated, and projecting through culture vessels slightly elevated off the print bed floor and into a scattering PEGDA solution can further exacerbate this. To characterize the resolution and effect of exposure time, we designed a virtual photomask of many features and patterned PEGDA with 40, 70, and 100 s exposures in 3.5 cm glass-bottomed Petri dishes (Figure 2A). As a note, we refer to exposure times for simplicity in this work, but Figure S1 shows the raw output power of the printer lamp in the 405 nm range, and exposure energy conversions can be defined by multiplying this output (~5.7 mW) by the exposure time. We then measured critical feature geometries and calculated the error relative to the target feature in the photomask. As shown in Figure 2B−D, we found the greatest accuracy was achieved using longer exposures around 70−100 s, which is highlighted in Figure 2D where we overlay outlines of patterns from the different exposures on top of a test rectangle pattern. Short exposures (40 s) led to patterns being too large, while longer exposures (70 and 100 s) led to patterns being somewhat smaller than the target, with percent errors often around 10−15% for patterns greater than 500 μm. For a final resolution characterization here, we also measured how closely we could space patterns to each other, again finding the most reliable performance at 100 s of exposure (Figure S2A and B).

As this is a variant of 2.5D lithography, we also characterized the gel height as a function of the exposure time and found a roughly linear relationship between maximum gel thickness and exposure time (Figures 2 E and F) but with relatively curved sidewalls (likely from the lack of collimation, 3D polymerization dynamics, and light scattering). Briefly, longer exposure times correspond to thicker gel layers, which can be used to control the substrate depth if desired.

3.3. Calibrations and Shape Corrections. Some deviation between the photomask and printed pattern is expected given the nature of the setup and the cost, but we wanted to demonstrate that this deviation could be empirically calibrated and corrected via a simple transfer function to reliably produce far more precise structures than might be expected. To demonstrate this, we chose to pattern circles of different sizes, as the radial symmetry of a circle and isotropic polymerization should make edge effects more pronounced (Figure 3A). Here, we patterned a series of descending circular openings and measured and fit a correspondence between a diameter in the photomask and an actual patterned diameter. Using this mapping, we were able to demonstrate precise and reproducible patterning of circles down to at most ~100 μm if we set the mask diameter to 600 μm and the exposure to 100 s (Figure 3B). A variety of settings can be adjusted to alter this correspondence, but the fact that such a clean calibration can be generated means that any user can quickly generate a correction curve for a given set of target patterns to allow for precise and rapid patterning. Moreover, this demonstrates surprisingly small pattern sizes for such a low-cost, high-throughput approach.

Importantly, the ability to create arbitrary photomasks using an LCD display enables a more advanced shape correction method for more complex shapes with variable curvatures. A clear example of where this would be useful is the rectangular patterns in Figure 2, where it is obvious that the 90° corners are all significantly rounded. The problem is easily stated: longer exposure times are important for reducing rectilinear dimension errors (Figure 2; e.g., width/length errors), but this comes at the cost of overpolymerization and rounding the corners (Figures 3C and D; yellow). This is likely because corners essentially concentrate the photopolymerization process, as the adjacent edges both contribute to the polymerization boundary. We hypothesized that we could compensate for this by artificially adjusting the radius of curvature at the corners. We demonstrated this approach by comparing the results from illumination with photomasks of pure rectangles to those masks where each corner was replaced with a circular contour to compensate for boundary growth (Figures 3C and D). This technique worked well and redirected the corner polymerization such that a sharp corner formed, allowing shapes with higher curvatures to be reproduced accurately.

3.4. Validation of Patterning Stability and Biocompatibility Using 2D and 3D Stem Cell Structures. Finally, we demonstrated how this rapid, inexpensive, and high-throughput method can be combined with popular and complex tissue engineering and patterning approaches. In this case, we aimed to engineer the self-organization of cells into complex structures reminiscent of gastrulation and

https://doi.org/10.1021/acsomega.4c06539
ACS Omega 2024, 9, 43808−43816

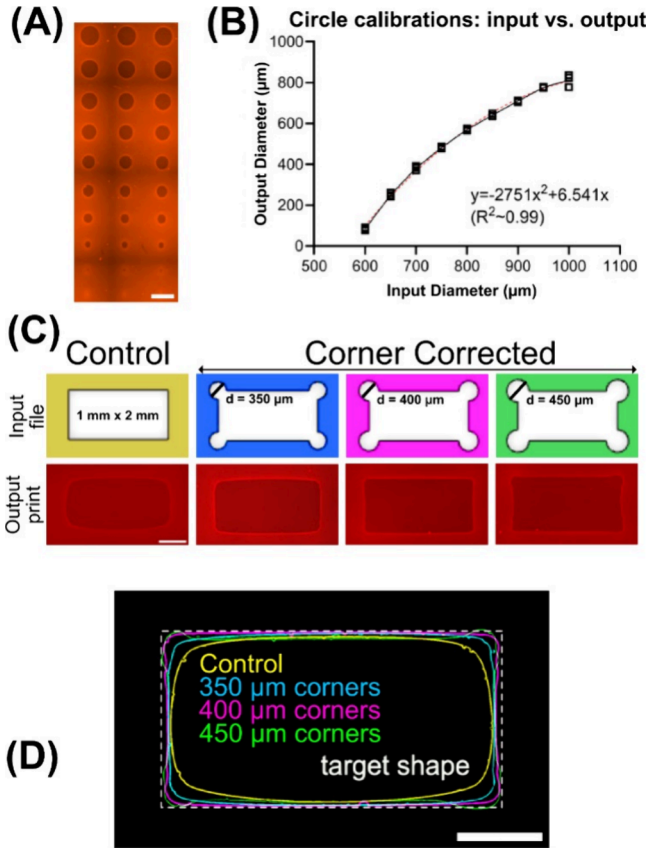

Figure 3. Patterning calibration curve and shape correction. (A) Epifluorescence image of circle patterns in varying sizes (1000−600 μm), with three replicates, printed with exposure time of 100 s. Scale bars: 1000 μm. (B) Circle patterning calibration curve between the diameter in the photomask (input diameter) and the patterned diameter (output diameter). (C) Rectangular patterns with circular corners of varying diameters as input files for shape correction testing. Epifluorescence images (contrast enhanced for clarity) of the printed rectangular patterns (output print) with sharp corners as the target shape. Scale bar: 500 μm. (D) Overlay of XY top-down edge profiles of representative rectangles printed with corrected corners. The white dotted line represents the targeted design size. Scale bar: 500 μm.

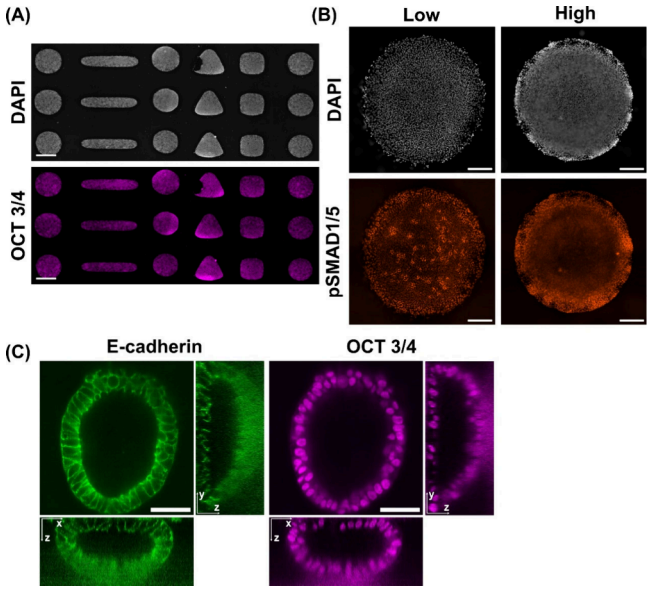

Figure 4. Validation of PEGDA hydrogel biocompatibility through 2D and 3D stem cell structures. (A) Immunofluorescence image of hiPSC patterned within a printed PEGDA hydrogel in various geometries. Cells were stained for the nucleus (top) and the OCT 3/4 pluripotency marker (bottom). Scale bars: 1 mm. (B) Immunofluorescence image of hiPSC 1 mm circle micropatterned colonies seeded at low (left, ~3000 cells/mm^2) and high densities (right, ~1000 cells/mm^2). Cells were stained for the nucleus (top) and pSMAD 1/5 (bottom). Scale bar: 200 μm (C) Epifluorescence images of E-cadherin (left) and OCT 3/4 immunostaining (right) of lumenized, or hollowed, 3D hiPSC structures. Scale bar: 50 μm.

lumenization[3,20,21] that are typically created using expensive and low-throughput patterning methods. Here, we printed patterns in various geometries, followed by laminin incubation, for culturing human induced pluripotent stem cells (hiPSCs) (Figure 4A). We first ensured that our materials and patterning method did not induce spontaneous differentiation, which we proved by showing that cells remain "positive" for the OCT3/4 pluripotency marker that proves the cells are still capable of differentiation (Figure 4A). After confirming the pluripotency of patterned hiPSCs, we induced differentiation by introducing bone morphogenetic protein 4 (BMP4) morphogen into the culture media to mimic the gastrulation environment. As previously reported,[22] the sensitivity of patterned stem cell colonies to BMP4 varied depending on their position in the micropattern at higher seeding densities, whereas this spatial sensitivity diminished at lower seeding densities. We successfully replicated this result by creating micropatterned hiPSC colonies with different cell seeding densities and immunostained them with an early differentiation marker, pSMAD 1/5. The signal of pSMAD 1/5 was uniformly distributed at lower seeding densities, while it became restricted to the colony edge as seeding density increased (Figure 4B). This means that the seeding density and therefore the spatial BMP responses can be easily calibrated with our patterning strategy.

Next, we demonstrated the high-throughput reproducible fabrication of complex hollow 3D tissues that recapitulate aspects of neurulation, where the hollow neural tube spontaneously develops. These engineered neural tubes are of great interest and can be differentiated downstream to "neuruloids" and recapitulate neural tube folding *in vitro*, upon neural induction.[21,23] We were able to demonstrate the key lumenization (hollowing) step here by patterning many discrete islands of laminin, culturing 2D hiPSC colonies, and then introducing a 3D Matrigel gel matrix on top of the colonies to induce lumen formation (Figure 4C). Again, these structures maintained their pluripotency, which is key for future differentiation steps, as shown by a positive OCT3/4 stain (Figure 4C).

3.5. Cell-Adhesive Biopolymer Patterning. The gently curved 3D surfaces we observed in projection-patterned PEGDA prompted us to replace the PEGDA with a common bioactive polymer, gelatin methacrylate (GelMA). This allowed us to explore whether we could get cells to adhere to complex 3D topographies rather than be excluded by them. GelMA is a widely used photopolymer for biological studies.[24] It mimics the ECM microenvironment, provides unique biocompatibility and cell-adhesiveness, and makes hydrogels with modular physicochemical properties.[25] Photopatterning is a popular approach for defining bioactive surfaces with both natural and synthetic polymers, and our system should be adaptable for a variety of these inks.[26,27] Such biomaterial

https://doi.org/10.1021/acsomega.4c06539
ACS Omega 2024, 9, 43808−43816

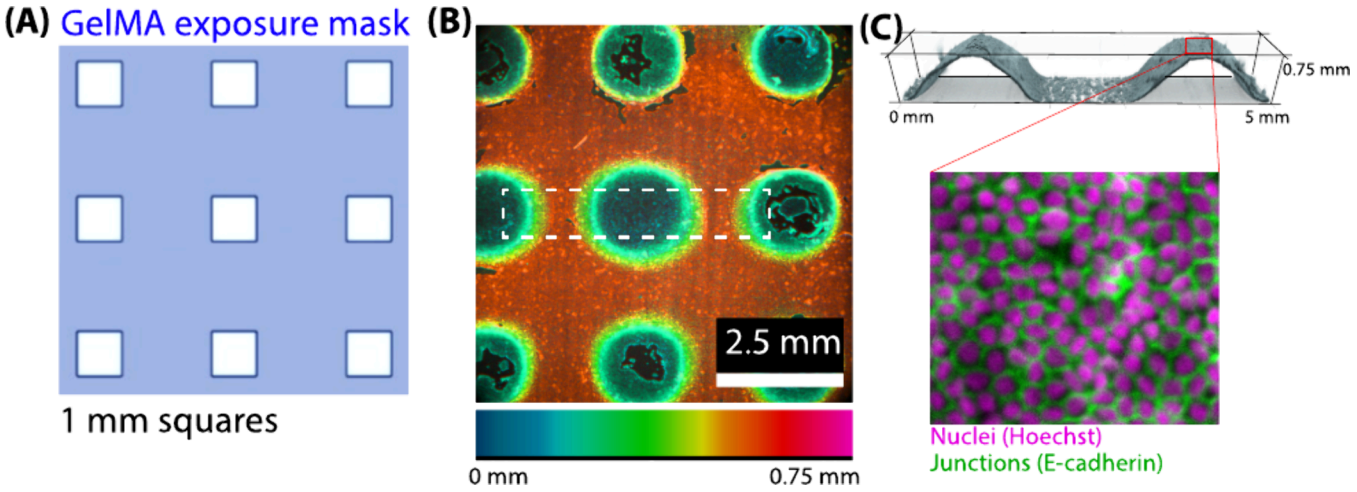

Figure 5. Validation of GelMA patterning: (A) Photomask for GelMA printing to generate 3D patterns. (B) Depth-coded topographic map of the MDCK tissue on a 3D GelMA pattern. The image represents the *z*-depth of the patterned tissue. (C) Image representing the 3D MDCK monolayer grown on GelMA. The 3D image was generated using Agave software. The inset image shows the monolayer tissue with nuclear stain and E-cadherin junctions.

surfaces are commonly used in studies on tissue curvature and for stem cell niche engineering.[28,29] Here, we used commercially produced GelMA (see Materials and Methods) and tested exposure patterns similar to what we had validated with PEGDA. Specifically, we evaluated a "waffle grid" that ought to produce tall ridges surrounding deep valleys, as shown in Figure 5a. We initially found that GelMA itself was not sufficiently cell-adhesive to anchor monolayer cultures, so we first incubated the GelMA in 50 μg/mL collagen (see Materials and Methods), which promoted better adhesion over 10 days of culture of our MDCK epithelial tissue model. Figure 5b shows the resulting depth-coded topographic map of the resulting tissue. The first thing we noted was that GelMA polymerization also exhibits increased corner polymerization, resulting in circular valleys rather than square profiles (see the blue vs red zones in Figure 5b). Notably, GelMA exhibited different patterning performance than PEGDA, and would require additional optimization if specific resolution constraints were required. We hypothesize this is due to a combination of different photochemistry and altered light scattering in GelMA relative to PEGDA.[30] We also noted significantly thicker polymerization zones in the *z*-axis, with these GelMA patterns extending up to nearly 750 μm in height, resulting in significant three-dimensionality of the patterned monolayer, as shown in the profile and monolayer inset in Figure 5C. This demonstration was a brief evaluation of the suitability for other biopolymers. While significant development work would be needed to tune this for a specific application, it is promising that the method works overall and offers a unique way to produce continuous 3D topography, although this is not expected to compete with a commercial bioprinter.

4. DISCUSSION AND CONCLUSION

The method described here is exciting because of its combination of simplicity, speed, low cost, and throughput. It demonstrates certain patterns down to 100 μm while also allowing nearly massive continuous tissue patterns across macroscale areas up to the size of a whole plate. The process requires merely pipetting a photopolymerizable inert gel into the culture regions of a dish or plate and placing the substrate on a budget resin printer before exposing it to a virtual photomask in 405 nm light. The rate of the patterning process is independent of the sample size, and an entire 96 well-plate can be patterned in <2 min. Moreover, it is worth mentioning both that the printer we used cost <$400 (less than we spent on the PEGDA or GelMA ink for this study) and that even more capable printers with higher resolution and brighter LCD systems have been released for the same price since we began this study. As a final point here, an added benefit to equipping a laboratory for this process is that the 3D printer can be converted back to a fully functional high-resolution resin 3D printer within just a few minutes, which further reduces the risk of equipping a laboratory for this process because our process does not damage the base 3D printer.

There are obvious limitations to such a low-cost process. The most obvious is that some work needs to be done upfront to calibrate and tune the photomask shapes when complex features are involved. This is primarily due to the relatively low power-density (requiring long exposures), lack of perfect collimation, and 3D polymerization dynamics (possibly amplified with long exposures). However, our method is not intended to compete with ultraprecise, lower-throughput, and more expensive approaches, and we have demonstrated several general calibration and correction methods that can be tuned for any given printer/resin system. An additional limitation is that the best performance involves using glass-bottom dishes, which can be more expensive than plastic dishes. With plastic dishes, the plastic base tends to be ∼10× thicker than an equivalent glass coverslip base, so light scattering in the plastic and collimation issues are significantly worsened. That said, this is a problem for any bottom-illuminated photopatterning approaches. Despite its limitations, our method occupies an important niche of cost, scale, and speed that is not accessible with other techniques at present.

There were a number of limitations that we observed in our approach, although they did not affect the general utility. Specifically, we observed dimensional errors of 10−15% in printing accuracy that we attributed to light scattering and photopolymerization dynamics (e.g., rounded corners), which are known to affect print accuracy.[30] Future optimization could evaluate photoabsorbers, which can reduce lateral scattering.[30,31] Hardware optimization can also improve the future

https://doi.org/10.1021/acsomega.4c06539
ACS Omega 2024, 9, 43808−43816

performance. For instance, monochrome LCD masks are reaching increasingly higher resolutions with smaller pixels, and pairing these masks with improved collimated 405 nm light sources will likely result in significant accuracy and speed improvements.

The foundation we present here encourages a number of interesting next steps. For instance, we suspect that dynamically shaping the photomask over time (e.g., making a circular mask larger or smaller over time) might reduce overpolymerization and result in straighter edges and high-aspect-ratio microwells. Such tuning is also needed for more specific patterning of cell-adhesive materials, as we demonstrated with GelMA. However, as the technique is low-cost and allows high-throughput iteration, there is little risk to exploring it, so we expect it to be much easier to adopt and test than other technologies in this space.

■ ASSOCIATED CONTENT

Supporting Information

The Supporting Information is available free of charge at https://pubs.acs.org/doi/10.1021/acsomega.4c06539.

Power measurements of the LCD screen, resolution characterization of PEGDA hydrogel, epifluorescence images of hydrogel, and percentage error graph (PDF)

■ AUTHOR INFORMATION

Corresponding Author

Daniel J. Cohen − *Department of Mechanical and Aerospace Engineering, Princeton University, Princeton, New Jersey 08544, United States*; Email: danielcohen@princeton.edu

Authors

Anamika Singh − *Department of Mechanical and Aerospace Engineering, Princeton University, Princeton, New Jersey 08544, United States*; orcid.org/0009-0005-0833-9839

Youn Kyoung Cho − *Department of Chemical and Biological Engineering, Princeton University, Princeton, New Jersey 08544, United States*; orcid.org/0009-0007-7190-1964

Complete contact information is available at: https://pubs.acs.org/10.1021/acsomega.4c06539

Author Contributions

#A.S. and Y.C. contributed equally to this work. Conceptualization: A.S., Y.C., D.J.C. Formal Analysis: A.S., Y.C. Funding acquisition: D.J.C. Methodology: A.S., Y.C., D.J.C. Project administration: D.J.C. Writing−original draft: A.S., Y.C., D.J.C. Writing−review and editing: A.S., Y.C., D.J.C.

Notes

The authors declare no competing financial interest.

■ ACKNOWLEDGMENTS

This work was funded by NIH NIGMS 6R35GM133574. The authors would like to acknowledge Isaac Breinyn for his help with image acquisition and generating production images. The work reported here has been duly filed for a patent with application number 63/656,846.

■ REFERENCES

(1) D'Arcangelo, E.; McGuigan, A. P. Micropatterning strategies to engineer controlled cell and tissue architecture in vitro. *BioTechniques* **2015**, *58*, 13−23.

(2) Blin, G. Quantitative developmental biology in vitro using micropatterning. *Development* **2021**, *148*, No. dev186387.

(3) Fu, J.; Warmflash, A.; Lutolf, M. P. Stem-cell-based embryo models for fundamental research and translation. *Nat. Mater.* **2021**, *20*, 132−44.

(4) Molina, A.; Scheibel, T.; Humenik, M. Nanoscale Patterning of Surfaces via DNA Directed Spider Silk Assembly. *Biomacromolecules* **2019**, *20*, 347−52.

(5) Xie, C.; Sun, W.; Lu, H.; Kretzschmann, A.; Liu, J.; Wagner, M.; Butt, H.-J.; Deng, X.; Wu, S. Reconfiguring surface functions using visible-light-controlled metal-ligand coordination. *Nat. Commun.* **2018**, *9*, 3842.

(6) Laurent, J.; Blin, G.; Chatelain, F.; Vanneaux, V.; Fuchs, A.; Larghero, J.; Théry, M. Convergence of microengineering and cellular self- confocal with a 2x objeorganization towards functional tissue manufacturing. *Nat. Biomed Eng.* **2017**, *1*, 939−56.

(7) Seo, J.; Shin, J.-Y.; Leijten, J.; Jeon, O.; Camci-Unal, G.; Dikina, A. D.; Brinegar, K.; Ghaemmaghami, A. M.; Alsberg, E.; Khademhosseini, A. High-Throughput Approaches for Screening and Analysis of Cell Behaviors. *Biomaterials* **2018**, *153*, 85−101.

(8) Perl, A.; Reinhoudt, D. N.; Huskens, J. Microcontact Printing: Limitations and Achievements. *Adv. Mater.* **2009**, *21*, 2257−68.

(9) You, J.; Heo, J. S.; Kim, H. O.; Kim, E. Direct photo-patterning on anthracene containing polymer for guiding stem cell adhesion. *Biomater Res.* **2016**, *20*, 26.

(10) Yin, H.; Ding, Y.; Zhai, Y.; Tan, W.; Yin, X. Orthogonal programming of heterogeneous micro-mechano-environments and geometries in three-dimensional bio-stereolithography. *Nat. Commun.* **2018**, *9*, 4096.

(11) Toh, C. R.; Fraterman, T. A.; Walker, D. A.; Bailey, R. C. Direct Biophotolithographic Method for Generating Substrates with Multiple Overlapping Biomolecular Patterns and Gradients. *Langmuir* **2009**, *25*, 8894−8.

(12) Song, Y. The poly-thymine based DNA photolithography onto electrostatic coupling substrates. *Materials Science and Engineering: C* **2020**, *111*, No. 110795.

(13) Strale, P.-O.; Azioune, A.; Bugnicourt, G.; Lecomte, Y.; Chahid, M.; Studer, V. Multiprotein Printing by Light-Induced Molecular Adsorption. *Adv. Mater.* **2016**, *28*, 2024−9.

(14) Choi, J. R.; Lee, J. H.; Xu, A.; Matthews, K.; Xie, S.; Duffy, S. P.; Ma, H. Monolithic hydrogel nanowells-in-microwells enabling simultaneous single cell secretion and phenotype analysis. *Lab Chip* **2020**, *20*, 4539−51.

(15) Yang, W.; Yu, H.; Li, G.; Wei, F.; Wang, Y.; Liu, L. Mask-free fabrication of a versatile microwell chip for multidimensional cellular analysis and drug screening. *Lab Chip* **2017**, *17*, 4243−52.

(16) Milton, L. A.; Viglione, M. S.; Ong, L. J. Y.; Nordin, G. P.; Toh, Y.-C. Vat photopolymerization 3D printed microfluidic devices for organ-on-a-chip applications. *Lab Chip* **2023**, *23*, 3537−60.

(17) Zhu, Y.; Sazer, D.; Miller, J. S.; Warmflash, A. Rapid fabrication of hydrogel micropatterns by projection stereolithography for studying self-organized developmental patterning. *PLoS One* **2021**, *16*, No. e0245634.

(18) Fairbanks, B. D.; Schwartz, M. P.; Bowman, C. N.; Anseth, K. S. Photoinitiated polymerization of PEG-diacrylate with lithium phenyl-2,4,6-trimethylbenzoylphosphinate: polymerization rate and cytocompatibility. *Biomaterials* **2009**, *30*, 6702−7.

(19) Shafique, H.; Karamzadeh, V.; Kim, G.; Shen, M. L.; Morocz, Y.; Sohrabi-Kashani, A.; Juncker, D. High-resolution low-cost LCD 3D printing for microfluidics and organ-on-a-chip devices. *Lab Chip* **2024**, *24*, 2774−90.

(20) Warmflash, A.; Sorre, B.; Etoc, F.; Siggia, E. D.; Brivanlou, A. H. A method to recapitulate early embryonic spatial patterning in human embryonic stem cells. *Nat. Methods* **2014**, *11*, 847−54.

(21) Karzbrun, E.; Khankhel, A. H.; Megale, H. C.; Glasauer, S. M. K.; Wyle, Y.; Britton, G.; Warmflash, A.; Kosik, K. S.; Siggia, E. D.; Shraiman, B. I.; Streichan, S. J. Human neural tube morphogenesis in vitro by geometric constraints. *Nature* **2021**, *599*, 268−72.

(22) Etoc, F.; Metzger, J.; Ruzo, A.; Kirst, C.; Yoney, A.; Ozair, M. Z.; Brivanlou, A. H.; Siggia, E. D. A Balance between Secreted Inhibitors and Edge Sensing Controls Gastruloid Self-Organization. *Dev Cell* **2016**, *39*, 302−15.
(23) Haremaki, T.; Metzger, J. J.; Rito, T.; Ozair, M. Z.; Etoc, F.; Brivanlou, A. H. Self-organizing neuruloids model developmental aspects of Huntington's disease in the ectodermal compartment. *Nat. Biotechnol.* **2019**, *37*, 1198−208.
(24) Piao, Y.; You, H.; Xu, T.; Bei, H.-P.; Piwko, I. Z.; Kwan, Y. Y.; Zhao, X. Biomedical applications of gelatin methacryloyl hydrogels. *Engineered Regeneration* **2021**, *2*, 47−56.
(25) Xiang, L.; Cui, W. Biomedical application of photo-crosslinked gelatin hydrogels. *J. Leather Sci. Eng.* **2021**, *3*, 3.
(26) Zhu, S.; Tang, Y.; Lin, C.; Liu, X. Y.; Lin, Y. Recent Advances in Patterning Natural Polymers: From Nanofabrication Techniques to Applications. *Small Methods* **2021**, *5*, No. e2001060.
(27) van Bochove, B.; Grijpma, D. W. Photo-crosslinked synthetic biodegradable polymer networks for biomedical applications. *Journal of Biomaterials Science, Polymer Edition* **2019**, *30*, 77−106.
(28) Wang, Y.; Gunasekara, D. B.; Reed, M. I.; DiSalvo, M.; Bultman, S. J.; Sims, C. E.; Magness, S. T.; Allbritton, N. L. A microengineered collagen scaffold for generating a polarized crypt-villus architecture of human small intestinal epithelium. *Biomaterials* **2017**, *128*, 44−55.
(29) Torras, N.; Zabalo, J.; Abril, E.; Carré, A.; García-Díaz, M.; Martínez, E. A bioprinted 3D gut model with crypt-villus structures to mimic the intestinal epithelial-stromal microenvironment. *Biomaterials Advances* **2023**, *153*, No. 213534.
(30) Goodarzi Hosseinabadi, H.; Nieto, D.; Yousefinejad, A.; Fattel, H.; Ionov, L.; Miri, A. K. Ink material selection and optical design considerations in DLP 3D printing. *Applied Materials Today* **2023**, *30*, No. 101721.
(31) Grigoryan, B.; Paulsen, S. J.; Corbett, D. C.; Sazer, D. W.; Fortin, C. L.; Zaita, A. J.; Greenfield, P. T.; Calafat, N. J.; Gounley, J. P.; Ta, A. H.; Johansson, F.; Randles, A.; Rosenkrantz, J. E.; Louis-Rosenberg, J. D.; Galie, P. A.; Stevens, K. R.; Miller, J. S. Multivascular networks and functional intravascular topologies within biocompatible hydrogels. *Science* **2019**, *364*, 458−64.

https://doi.org/10.1021/acsomega.4c06539
ACS Omega 2024, 9, 43808−43816